The Reaction-Limited Kinetics of Membrane-to-Surface Adhesion and Detachment
Author(s): M. Dembo, D. C. Torney, K. Saxman and D. Hammer
Source: *Proceedings of the Royal Society of London. Series B, Biological Sciences,* Vol. 234, No. 1274 (Jun. 22, 1988), pp. 55-83
Published by: Royal Society
Stable URL: http://www.jstor.org/stable/36290
Accessed: 30-04-2018 22:03 UTC

Proc. R. Soc. Lond. B **234**, 55–83 (1988)
Printed in Great Britain

The reaction-limited kinetics of membrane-to-surface adhesion and detachment

By M. Dembo, D. C. Torney, K. Saxman and D. Hammer

Theoretical Biology and Biophysics (*T*-10), *Theoretical Division*, *Los Alamos National Laboratory*, *Los Alamos*, *New Mexico* 87545, *U.S.A.*

(*Communicated by J. D. Murray, F.R.S.* – *Received* 22 *September* 1987)

Biological adhesion is frequently mediated by specific membrane proteins (adhesion molecules). Starting with the notion of adhesion molecules, we present a simple model of the physics of membrane-to-surface attachment and detachment. This model consists of coupling the equations for deformation of an elastic membrane with equations for the chemical kinetics of the adhesion molecules. We propose a set of constitutive laws relating bond stress to bond strain and also relating the chemical rate constants of the adhesion molecules to bond strain.

We derive an exact formula for the critical tension. We also describe a fast and accurate finite difference algorithm for generating numerical solutions of our model. Using this algorithm, we are able to compute the transient behaviour during the initial phases of adhesion and detachment as well as the steady-state geometry of adhesion and the velocity of the contact.

An unexpected consequence of our model is the predicted occurrence of states in which adhesion cannot be reversed by application of tension. Such states occur only if the adhesion molecules have certain constitutive properties (catch-bonds). We discuss the rational for such catch-bonds and their possible biological significance. Finally, by analysis of numerical solutions, we derive an accurate and general expression for the steady-state velocity of attachment and detachment.

As applications of the theory, we discuss data on the rolling velocity of granulocytes in post-capillary venules and data on lectin-mediated adhesion of red cells.

Introduction

The 'peel test' is an important method of assessing the performance and characteristics of adhesives used in industrial and engineering applications. To do the peel test, one half of a long strip of a flexible membrane of known bending modulus is attached to a smooth surface by using various adhesives or methods of application. The test then consists of measuring the rate (length per unit time) at which the membrane is peeled off the surface when tension is applied to the free end. Alternatively, one can measure the tension generated at a given rate of peeling.

If one wishes to glue two parts together in a reliable manner, then one has to decide between various means at hand, and the peel test can frequently give an answer in a purely empirical fashion and without the need for any deep analysis.

On the other hand, in the context of cell adhesion, one wishes to use the peel test as a scientific means of exploring the biochemical and biophysical basis of adhesion. This means that it is helpful to develop quantitative formulations of various hypothetical models of adhesion and to compare experimental results with the predictions of these models.

Since the early studies of McEwan & Taylor (1966), several authors have developed continuum models of the peel test as used in engineering (recent examples are Crocombe & Adams (1981, 1982) and Yamamoto *et al.* (1975); also, see review by Krenceski *et al.* (1986)). These models view the adhesive layer separating the membrane from the surface as a continuum that obeys more or less complicated viscoelastic or viscoplastic constitutive relations. Numerical methods are used to compute the detailed distribution of stresses that are developed in the adhesive during the peel test. Various modes of failure of the adhesive are associated with certain critical values of the stress.

These models cannot be carried over to a biological setting without some modification. In part, this is because of the very small size of the gap separating an adherent cell from the surface to which it binds. Because this gap is of the same order of magnitude as the size of typical cell surface glycoproteins (cell adhesion molecules included), it is neither appropriate nor possible to characterize the intervening material as a continuum with respect to a curvilinear axis that spans the cell-to-surface gap. Additional motivation for rejecting the concept of a continuous 'adhesive' comes from the fact that there are usually only a few (10^3–10^6) adhesion molecules per cell and from the fact that there are many other components of the glycocalyx in the cell-to-surface gap. These latter components may have nothing to do with adhesion or, in fact, they may work against adhesion either passively (by taking up space) or actively (by mediating repulsive interactions) (Bell *et al.* 1984; Bongrand & Bell 1984).

The discrete molecular basis of cell–cell or cell–surface bonding has been well recognized in previous models of these phenomena. Bell and co-workers (Bell *et al.* 1984; Torney *et al.* 1986; Dembo & Bell 1987) have proposed and analysed several detailed models of membrane-to-membrane and membrane-to-surface adhesion. These models were primarily concerned with the balance between bonding enthalpy, repulsive potentials, and mixing entropy; the finite bending rigidity of the cell membrane was modelled by placing an upper constraint on the area of contact. These models did not consider the effect of tension applied to the membrane and were restricted to states of thermodynamic equilibrium.

Evans (1985*a*, *b*), has discussed models that include the effects of bending rigidity and tension but without considering repulsive forces or mixing entropy. Evans has considered states that depart from thermal equilibrium but only if such states are kinetically trapped (i.e. only if they are in mechanical equilibrium).

In the present work we shall attempt to build on both these previous contributions. Our main purpose is to develop an analytical expression for the steady-state velocity of peeling as measured in a biological version of the peel test.

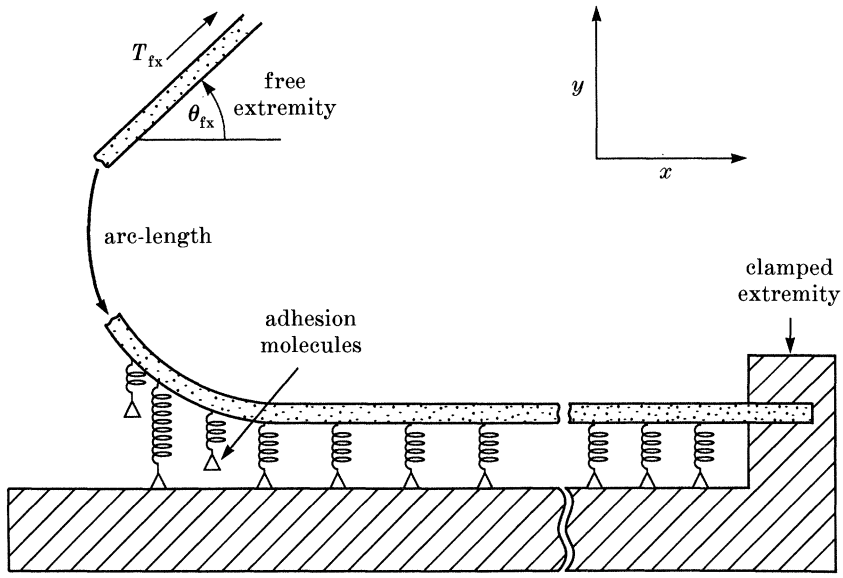

FIGURE 1. The geometry of membrane-to-surface adhesion is illustrated. The surface to which the membrane binds is taken as coincident with the X-axis of Cartesian coordinates. Position along the contour of the membrane is tracked by the arc-length coordinate, s. At the free extremity ($s \to -\infty$), tension (T_{fx}) is applied to the membrane at a particular angle (θ_{fx}) with respect to the surface. At the clamped extremity ($s \to +\infty$) the membrane is firmly attached to the surface so as to prevent lateral slippage.

THE MODEL

Figure 1 shows the geometry of the peel test and introduces some basic notation. We take the surface to which the membrane binds as coincident with the X-axis of Cartesian coordinates in the laboratory frame. The position along the contour of the membrane is tracked by an arc length coordinate, s. The shape of the membrane at any instant of time, t, is specified by the locus of points $X(s,t)$, $Y(s,t)$. At one extremity, ($s \to -\infty$), tension is applied to the membrane at a specified orientation with respect to the surface. At the other extremity ($s \to +\infty$), we presume that the membrane is firmly clamped to the surface. The latter precaution is taken to ensure that the membrane cannot slip horizontally with respect to the surface.

Bonding between the membrane and the surface is presumed to be mediated by specific adhesion molecules. The surface density of free or unattached adhesion molecules is given by a function of arc length and time, $A_f(s,t)$; the density of consummated membrane-to-surface bridges is given by $A_b(s,t)$. The formation and breakage of cell-to-surface bonds at any position of the membrane is taken to be a reversible stochastic chemical rate process of the simple type

$$A_f \underset{K_r(Y)}{\overset{K_f(Y)}{\rightleftharpoons}} A_b. \tag{1}$$

As indicated by (1), the forward and reverse reaction rates (K_f and K_r) are functions (to be specified subsequently) of the vertical separation between the

membrane and the surface. In a more general theory these rate functions could also depend on the slope of the membrane with respect to the surface.

We shall restrict consideration to cases in which the adhesion molecules are anchored in the plane of the membrane (i.e. the molecules are not free to diffuse or slip in a lateral (fashion). In this event, the total density of adhesion molecules must be a fixed constant:

$$A_f(s,t)+A_b(s,t)=A_{total}. \tag{2}$$

By using (2), the continuity equation for the bond density becomes

$$\partial_t A_b(s,t)=K_f(Y)\,A_{total}-(K_r(Y)+K_f(Y))\,A_b(s,t). \tag{3}$$

A point on the membrane is said to be in 'contact' with the surface if the bond density at this point is greater than or equal to some small positive quantity called the 'contact threshold'. We denote the contact threshold by $A_{b,c}$. The first point of contact between the membrane and the surface (denoted by P_c) is defined to be the smallest value of s such that $A_b(s,t)=A_{b,c}$.

Suppose that we choose initial conditions such as P_c exists and is at the origin of arc length $t=0$. Because bonds can form and break, P_c will in general be a function of time. We have not attempted a rigorous mathematical proof; nevertheless, we find by direct numerical construction that P_c is both continuous and differentiable. Given that this is so, the peeling velocity can be defined to be the first-time derivative of P_c,

$$V_{pl}(t)=\partial_t P_c(t). \tag{4}$$

According to this equation, negative values of V_{pl} correspond to rates of bonding or annealing between the membrane and surface.

Our definitions of contact point and peeling velocity imply that both these quantities depend on the seemingly arbitrary choice of a value for the contact threshold. Fortunately, this is only true during the phase of peeling when the bond distribution and the shape of the membrane are changing rapidly (see Results). During this transient phase, different parts of the membrane move in different ways, and there is no absolute way to define the peeling rate in terms of a single quantity. The situation changes at large times once a steady or periodic process of peeling or annealing is achieved. If the process is a steady state, then it can be shown that the value of V_{pl} must become independent of the choice of contact threshold. If the process is periodic, then although the detailed wave-form could depend on $A_{b,c}$, the average of V_{pl} over one cycle is independent of contact threshold.

In our subsequent discussions when we refer to peeling rate we sometimes fail to state the value of the contact threshold with respect to which this quantity is defined. In such cases it should be understood that the peeling rate in question refers to a steady or periodic process. It is therefore independent of the choice of contact threshold.

Let us now adopt a frame of reference such that the contact point is synonymous with the origin of arc length:

$$\tilde{s}=s-P_c(t). \tag{5}$$

In the new coordinates, the peeling velocity appears explicitly as a virtual convection term in the continuity equation for the bond density

$$\partial_t A_b = V_{pl}\,\partial_{\tilde{s}} A_b + K_f A_{total} - (K_f + K_r) A_b. \tag{6a}$$

The instantaneous value of the peeling velocity now becomes explicit because in the new coordinates the bond density is always equal to the contact threshold at the origin:

$$V_{pl} = -(K_f A_f - K_r A_b)/(\partial_{\tilde{s}} A_b) \quad \text{at } \tilde{s} = 0. \tag{6b}$$

Given $K_f(Y)$ and $K_r(Y)$, (6*a*, *b*) constitute an explicit relation between the kinetics of bonding and the membrane shape. The converse relation must also be explicit. We therefore propose to adopt what is doubtless a very simplistic model of what may be called the 'bonding stress'. To this end, a cell-to-surface bond will be viewed as a simple Hookean spring with spring constant κ and λ. We think of these bonds as being stretched vertically between points on the membrane and the projection of these points on the surface below. In consequence, the normal and tangential components of the bonding stress on the membrane are

$$\sigma_{nor} = A_b \kappa (Y - \lambda)\,\partial_{\tilde{s}} X \tag{7a}$$

and

$$\sigma_{tan} = -A_b \kappa (Y - \lambda)\,\partial_{\tilde{s}} Y, \tag{7b}$$

respectively.

We shall henceforth assume that bonding stresses are the only distributed stresses of importance. We thus neglect forces due to shearing motions of surrounding viscous fluid, transmembrane pressure gradients and nonspecific repulsive or attractive potentials between the membrane and the surface (e.g. electrostatic and electrodynamic potentials). The treatment of these additional stresses can readily be accomplished but at considerable cost in terms of pedagogical clarity. In addition, one can show that in a certain sense frictional stresses (such as hydrodynamic stresses) are dominated by the bonding stresses when one is 'sufficiently close' to thermal equilibrium. This is simply because such stresses are proportional to the velocity of peeling.

For given normal and tangential stresses, it is well known that in the absence of inertia, the tension and curvature of a thin inextensible membrane are governed by the coupled nonlinear system (Evans & Skalak 1980; Evans 1985*a*):

$$\partial_{\tilde{s}}(T + 0.5 M_b C^2) = -\sigma_{tan}, \tag{8}$$

$$M_b \partial_{\tilde{s}}^2 C - CT = -\sigma_{nor}. \tag{9}$$

In these expressions, M_b is the modulus of bending, C is the curvature and T is the tension.

In addition to (8) and (9), we know by definition of the curvature that

$$\begin{aligned} C &= (\partial_{\tilde{s}} X)(\partial_{\tilde{s}}^2 Y) - (\partial_{\tilde{s}}^2 X)(\partial_{\tilde{s}} Y) \\ &= (\partial_{\tilde{s}}^2 Y)/(\partial_{\tilde{s}} X), \end{aligned} \tag{10}$$

and by definition of the arc length that

$$(\partial_{\tilde{s}} X)^2 + (\partial_{\tilde{s}} Y)^2 = 1. \tag{11}$$

To form a well posed mathematical system, (6*a*, *b*), (7*a*, *b*), (8), (9), (10) and (11) must be supplemented by appropriate boundary and initial conditions. At the free extremity of the membrane ($\tilde{s} \to -\infty$), we require,

$$\partial_{\tilde{s}} Y \to -\sin(\theta_{\mathrm{fx}}), \tag{12a}$$

$$C(\tilde{s}, t) \to 0 \tag{12b}$$

and

$$T(\tilde{s}, t) \to T_{\mathrm{fx}}, \tag{12c}$$

where θ_{fx} is the angle between the membrane and the surface at the free extremity and T_{fx} is the tension applied at the free extremity (see figure 1).

At the clamped extremity ($\tilde{s} \to +\infty$), we require the gap between membrane and surface be such that normal stresses on the membrane approach zero. We also require that the membrane be parallel to the surface. Thus

$$Y(\tilde{s}, t) \to \lambda \tag{13a}$$

and

$$\partial_{\tilde{s}} Y \to 0. \tag{13b}$$

It is notable that according to our definition, θ_{fx} is the included angle between the clamped and the free extremities of the membrane. This angle is measured when one is a very large distance away from the region of membrane bending and should not be confused with the contact angle between liquids or between a liquid and a solid. The latter quantities refer to the actual angle at which material surfaces join.

As a consequence of the boundary conditions, it can be seen from (6*a*) that at sufficiently long times

$$A_{\mathrm{b}}(\tilde{s}, t) \to 0, \tag{14}$$

as $\tilde{s} \to -\infty$. By the same token, if we let

$$K_{\mathrm{eq}} = K_{\mathrm{f}}(\lambda)/K_{\mathrm{r}}(\lambda) \tag{15a}$$

be the equilibrium constant for formation of unstressed bonds, then

$$A_{\mathrm{b}}(\tilde{s}, t) \to A_{\mathrm{tot}} K_{\mathrm{eq}}/(1+K_{\mathrm{eq}}) = A_{\mathrm{b,eq}} \tag{15b}$$

as $\tilde{s} \to +\infty$.

As far as initial conditions are concerned, we shall restrict consideration to the case where the starting bond distribution is a two-step function of the form

$$\left.\begin{aligned} A_{\mathrm{b}}(\tilde{s}, 0) &= 0 && \text{if } \tilde{s} < 0, \\ A_{\mathrm{b}}(\tilde{s}, 0) &= A_{\mathrm{b,c}} && \text{if } \tilde{s} = 0, \\ A_{\mathrm{b}}(\tilde{s}, 0) &= A_{\mathrm{b,eq}} && \text{if } \tilde{s} > 0. \end{aligned}\right\} \tag{16}$$

This function is the simplest choice if one requires that the contact point exist at $t = 0$ and that the limiting behaviour at $\tilde{s} = +$ and $-\infty$ be appropriate.

The specification of our model is now almost complete, but it still remains for us to provide an explicit form of the relation between the rate constants, K_{f} and K_{r}, and the size of the cell-to-surface gap (Y). The starting point for deriving this relation must be a clear appreciation of the need for thermodynamic consistency between any such relation and the simple Hookean spring concept of the bonding

stress. The standard-state free energy of a Hookean spring stretched or compressed until it has end-to-end length Y, can be expressed in the form

$$G_h = G_{h0} + 0.5\kappa(Y-\lambda)^2, \tag{17a}$$

where G_{h0} is the standard state free energy of the unstretched spring. This means that the equilibrium constant for formation of a stretched bond has the form

$$K_f(Y)/K_r(Y) = \exp(-G_h/B_z) = K_{eq}\exp(-0.5\kappa((Y-\lambda)^2)/B_z), \tag{17b}$$

where B_z is the product of Boltzmann's constant and the absolute temperature and K_{eq} is as given by (15*a*).

Equation (17*b*) means that if we specify K_f, then K_r is determined *en passant*. The former specification can be accomplished if one makes good use of the Arrhenius (or transition state) theory of chemical reaction rates. To apply the transition state theory we need only remark on two facts. First, the free energy of an unattached adhesion molecule is a constant that does not depend on the gap separating the molecule from its potential attachment site. Secondly, the standard state free energy of the transition state for formation of a stretched (or compressed) bond will have the same Hookean form given by (17*a*). Of course, the base energy of the unstressed transition state as well as the spring constant and rest length of the transition state will be somewhat different from the corresponding quantities for the final bonded state. For simplicity we shall assume that the differences between the transition state and the bonded state can be described by a change in the spring constant only.† This leads immediately to the expression

$$K_f(Y) = K_f(\lambda)\exp\{-0.5\kappa_{ts}((Y-\lambda)^2)/B_z\}, \tag{18}$$

where κ_{ts} is spring constant of the transition state.

One may now combine (17*b*) and (18) to obtain the consistent expression for K_r:

$$K_r(Y) = K_r(\lambda)\exp\{0.5(\kappa-\kappa_{ts})(Y-\lambda)^2/B_z\}. \tag{19}$$

If the transition state is a stiffer spring than the bound state (i.e., if $(\kappa_{ts}-\kappa) > 0$,) then (19) implies that the rate of disruption of a highly stretched bond will actually be slower than the rate for disruption of an unstressed bond. This at first might seem rather implausible, but in actuality it is easy to construct molecular models of well-to-substratum bonds that will give this behaviour. The basic mechanism of such models is similar to that of the child's toy known as the 'finger-prison'.‡ In other words, the stress created by stretching the bond acts as a lever to lock the bonding groups more tightly together.

The predictions of our model depend very strongly on whether or not the bonds are capable of finger-prison type of behaviour. This property of bonds is so fundamental that it is useful to distinguish two entirely different types of bonds: catch-bonds and slip-bonds. All bonds for which $K_r(Y)$ approaches zero as Y approaches infinity are said to be catch-bonds; otherwise the bonds are said to be

† We shall consider an alternative hypothesis in Appendix 1.

‡ A finger-prison is a flexible tube made of helically wound filaments. The object will admit entrance of a finger, but it collapses and resists when egress is attempted.

slip-bonds. From (19) it is apparent that any bonds for which κ_{ts} is strictly greater than κ will be catch-bonds. Bonds for which κ_{ts} is exactly equal to κ qualify as slip-bonds.

The critical tension

The critical tension is the value of T_{fx} required to just overcome the tendency of the membrane to spread over the surface. In many systems this quantity has been measured experimentally (see Analysis of experiment).

We know of two ways to derive the exact analytic expression for the critical tension predicted by our model: an approach based on energy conservation and an approach based on horizontal force balance. We shall present the latter proof. An application of energy arguments, to obtain the same final result but in a somewhat different context, can be found in the Appendix of Evans (1985*a*).

According to our model, bonding stresses always act in the vertical direction. Thus the only horizontal forces acting on the membrane are due to the tensions acting on the free and clamped extremities. A simple free-body diagram will thus show that for horizontal forces to balance:

$$\lim_{\tilde{s}\to-\infty}(\partial_{\tilde{s}}X)T+\lim_{\tilde{s}\to+\infty}(\partial_{\tilde{s}}X)T=0.$$

If we now apply the boundary conditions, it follows that the tension at the clamped extremity is given by

$$T_{cx}=-\lim_{(\tilde{s}\to+\infty)}(\partial_{\tilde{s}}X)T=-T_{fx}\cos(\theta_{fx}). \tag{20}$$

Let us now turn to the continuity equation for A_b, (6*a*). If we assume steady state, then it is apparent that A_b can be expanded as power series in V_{pl}

$$A_b=a_{b0}+a_{b1}V_{pl}+a_{b2}V_{pl}^2+\dots. \tag{21}$$

Substituting into (6*a*), collecting powers of V_{pl} and using (17*b*), we find that

$$\left.\begin{aligned} a_{b0}&=\frac{A_{total}K_{eq}\exp\{-0.5(\kappa/B_z)(Y-\lambda)^2\}}{[1.0+K_{eq}\exp\{-0.5(\kappa/B_z)(Y-\lambda)^2\}]},\\ a_{b1}&=\frac{(\partial_{\tilde{s}}a_{b0})}{(K_r+K_f)},\end{aligned}\right\} \tag{22}$$

etc.

We now combine (21) with the expression for tangential stress (7*b*). Substitution of the resulting expression into the right-hand side of (8) yields:

$$O(V_{pl})=-a_{b0}\kappa(Y-\lambda)(\partial_{\tilde{s}}Y)+\partial_{\tilde{s}}(T+0.5M_bC^2). \tag{23}$$

Using (22) with the boundary conditions at the free extremity, we can integrate (23) from $-\infty$ to $\tilde{s}$. The result is:

$$A_{total}B_z\ln[1+K_{eq}\exp\{-0.5(\kappa/B_z)(Y-\lambda)^2\}]+0.5M_bC^2+T-T_{fx}=O(V_{pl}). \tag{24}$$

Next we take the limit of (24) as $\tilde{s} \to +\infty$ and apply (20) with the boundary conditions at the clamped extremity:

$$[1+\cos(\theta_{\mathrm{fx}})]T_{\mathrm{fx}} = A_{\mathrm{total}} B_{\mathrm{z}} \ln[1+K_{\mathrm{eq}}] + O(V_{\mathrm{pl}}). \tag{25}$$

Finally, because V_{pl} is zero at the critical tension, we have proved that:

$$T_{\mathrm{crit}} = \frac{B_{\mathrm{z}} A_{\mathrm{total}} \ln[1+K_{\mathrm{eq}}]}{(1+\cos(\theta_{\mathrm{fx}}))}. \tag{26}$$

If we regard θ_{fx} as analogous to the liqud–solid or liquid–liquid contact angle, then it can be seen that (26) has the same form as the classical Young equation (Adamson 1976). Continuing this analogy, the surface energy for bonding between the membrane and the surface is equal to the numerator on the right-hand side of (26). The only advantage of (26) is that the surface energy is given as an explicit function of the Boltzmann factor, the total density of adhesion molecules, and the equilibrium constant of the adhesion molecules: quantities subject to independent measurement.

It is important to realize that (26) neglects the contributions of non-specific attractive and repulsive potentials. Fortunately, it is possible to compute the consequences of these additional factors by a straightforward generalization of the arguments given above. We shall simply state the result and omit the detailed proof.

Let $\Gamma(Y)$ be the conservative work required to bring a unit area of membrane from infinite distance to vertical distance Y in the absence of bond formation. To compute the critical tension when Γ is non-zero, we must first examine the roots of the indicial equation

$$a_{\mathrm{b0}}(Y-\lambda)\kappa = -\partial_{\tilde{s}}\Gamma.$$

If no positive root of this equation exists, then the bonding stresses are unable to overcome the repulsive forces, and stable adhesion is not possible. In this event the concept of critical tension is meaningless. If a positive root, Y_{eq}, does exist, then:

$$T_{\mathrm{crit}} = \frac{\{A_{\mathrm{total}} B_{\mathrm{z}} \ln[1+K_{\mathrm{eq}} \exp(-0.5(\kappa/B_{\mathrm{z}})(Y_{\mathrm{eq}}-\lambda)^2)] - \Gamma(Y_{\mathrm{eq}})\}}{(1+\cos(\theta_{\mathrm{fx}}))}.$$

It can be seen from the above expressions that, in general, it will be safe to neglect non-specific forces only if the value of λ is large compared with the range of these forces. Because the *raison d'etre* of adhesion molecules is precisely to overcome repulsive forces, one has good teleological justification for suspecting that this will often be the case.

Numerical methodology

The formula for the critical tension is an exact analytical result and is very useful as far as it goes. However, because our model gives rise to a highly non-linear system of partial differential equations (PDEs), it seems inevitable that any really deep analysis must rest on the study of numerical solutions. Therefore it is necessary to compute numerical solutions that are highly reliable and accurate.

Furthermore, it is necessary to study many such solutions. This computational efficiency is extremely important.

The major challenge in numerically solving our model is the necessity of resolving structure over a very wide range of distance scales. The molecular scale is defined by the distance $\sqrt{B_z/\kappa}$: (i.e. by the strain required to raise the internal energy of a bond by one Boltzmann). At the other extreme, to apply the boundary conditions at $\tilde{s} = +$ and $-\infty$, one must resolve distances that are large compared with the radius of curvature of the membrane.

To overcome these difficulties, we utilize the fact that we are free to make the bond density at the contact point ($A_{b,c}$) as small as we wish. If the contact threshold is truly negligible, then we can ignore the bonding stresses on the portions of the membrane that lies to the left of the contact point, because the bond density at these points will be even smaller than the contact threshold. The result is that, for $\tilde{s} < 0$, one can partially integrate the system of equations that govern the membrane deformation and tension. We are thus able to replace the boundary conditions at $\tilde{s} \to -\infty$, by matching conditions at $\tilde{s} \leqslant 0$. The matching conditions are:

$$M_b(\partial_{\tilde{s}} C) = T_{fx}[(\partial_{\tilde{s}} X)\sin(\theta_{fx}) - (\partial_{\tilde{s}} Y)\cos(\theta_{fx})], \tag{27a}$$

$$T = -T_{fx}[(\partial_{\tilde{s}} Y)\sin(\theta_{fx}) + (\partial_{\tilde{s}} X)\cos(\theta_{fx})], \tag{27b}$$

$$0.5 M_b C^2 = T_{fx} - T. \tag{27c}$$

We now proceed to introduce a finite difference formulation of the model and solve the resulting nonlinear algebraic system by a relaxation method. The region $\tilde{s} > 0$ is divided into a large number of uniform segments. The number and length of these segments are adjustable numerical parameters. All fundamental quantities, bond densities, X and Y coordinates, as well as tensions, are edge-centred. In the continuity equation (6a) the backward Euler scheme is used for the time derivative, and upstream differencing with simple donor cell advection is used to discretize the virtual convection term. Given bond densities from the previous time step, a subroutine 'Boncalc' equation computes V_{pl} using (6b), and then does one cycle of an under-extrapolated Jacobi procedure for the linear system derived from the continuity equation. X and Y coordinates of the segment edges are regarded as fixed by this subroutine.

In a second subroutine, 'Tencalc', the tension at each segment edge is calculated by numerically integrating (8), subject to the appropriate matching condition at $\tilde{s} = 0$. This subroutine regards bond densities as well as X and Y coordinates as given.

In a third subroutine, 'Ycalc', Y coordinates of segment edges are refined by using the discretized forms of (9) and (10) with the appropriate boundary and matching conditions. The large banded matrix that results from this discretization is inverted by direct lower–upper (LU) decomposition. In Ycalc, X coordinates, tensions and bond densities are regarded as given.

In a final subroutine, 'Xcalc', the X coordinates of segment edges are adjusted by using (11) and the existing Y coordinates. This ensures that segment lengths are always completely fixed.

In each time step, Boncalc, Tencalc, Ycalc, and Xcalc are repeatedly executed

until a convergence criterion is satisfied. Then new bond densities are exchanged for old, and the time is incremented. The overall iterative process is stable provided the time step satisfies a Courant condition and is not too large compared with the characteristic relaxation time of the bonding reaction near $\tilde{s} = 0$. It is also necessary that the slope of the membrane at $\tilde{s} = 0$ does not approach very close to the vertical.

Before we present results that are based on the study of numerical computations obtained with this algorithm, it is necessary to discuss the nature of the controls and checks that we have conducted to convince ourselves that our numerical results are accurate. First, and most elementary, were checks of Cauchy convergence of the numerical method. This was studied by matched computations in which all parameters were held fixed except for the segment size, the number of segments to the right of the contact point, the contact density, the size of the time step and the convergence criterion for the iteration at each time step. For any given set of physical parameters, it was elementary to arrive at estimates of the aforementioned numerical parameters such that a further doubling of numerical accuracy results in only 1–2% change in steady-state peeling velocity. This level of accuracy was then routinely used.

The accuracy of those portions of the method that solve for the elastic deflection of the membrane at fixed bond distribution were independently confirmed by comparison with a class of approximate analytic solutions that are readily obtained in the linearized small deflection limit. Accuracy of the order of 1% was obtained.

Finally, a very important and independent check on the accuracy of the numerical method was its ability to give the right value of the critical tension and the right value of the clamping tension (20) and (26). For all parameters studied, numerical determinations of the critical tension were found to be remarkably accurate (better than 0.1%).

Information structure

Let us introduce a non-dimensional time variable:

$$\hat{t} = K_r(\lambda)\, t \tag{28a}$$

and non-dimensional arc length

$$\begin{aligned} \tilde{s} &= \tilde{s}(\kappa/B_z)^{\frac{1}{2}} \\ &= (s - P_c(t))\,(\kappa/B_z)^{\frac{1}{2}}. \end{aligned} \tag{28b}$$

The corresponding non-dimensional dependent variables are the non-dimensional curvature and coordinates of the membrane:

$$\hat{C} = C(B_z/\kappa)^{\frac{1}{2}}, \tag{29a}$$

$$\hat{X} = X(\kappa/B_z)^{\frac{1}{2}}, \tag{29b}$$

$$\hat{Y} = (Y - \lambda)\,(\kappa/B_z)^{\frac{1}{2}}; \tag{29c}$$

non-dimensional tension, $$\tilde{T} = T/T_{crit}; \tag{29d}$$

peeling velocity, $$\tilde{V}_{pl} = [V_{pl}/K_r(\lambda)]\,(\kappa/B_z)^{\frac{1}{2}}; \tag{29e}$$

and non-dimensional bond densities,

$$\hat{A}_b = A_b/A_{b,eq} \tag{29f}$$

and

$$\hat{A}_f = A_f/A_{b,eq}. \tag{29g}$$

After changing variables, it can be shown that for the above scaling, our model is governed by five independent non-dimensional groups. We will take these to be:

$$K_{eq} = K_f(\lambda)/K_r(\lambda), \tag{30a}$$

$$\beta = A_{total} B_z^2/(M_b \kappa), \tag{30b}$$

$$F_\kappa = (\kappa - \kappa_{ts})/\kappa, \tag{30c}$$

$$\theta_{fx}, \tag{30d}$$

and

$$\hat{T}_{fx} = T_{fx}/T_{crit}. \tag{30e}$$

Technically, one should also include the non-dimensional contact threshold,

$$\epsilon_c = A_{b,c}/A_{b,eq}, \tag{30f}$$

but this is really an artificial quantity that is introduced mainly for numerical convenience.

To do useful numerical studies it is helpful to have estimates of the applicable non-dimensional quantities. In the case of $\hat{\theta}_{fx}$ and $\hat{T}_{fx}$, such estimates are self-evident. One may also reasonably assume that the variation of stiffness of the adhesion molecules between transition state and bonded state (i.e., F_κ) is only a few percent. Other estimates of important parameters of our model for typical biological systems are shown in table 1.

TABLE 1. ESTIMATES OF PARAMETERS USED IN THE MODEL FOR TYPICAL BIOLOGICAL SYSTEMS

parameter	estimated value	unit
K_{eq}	10^{-4} to 10^{9}	—
A_{total}	10^{9} to 10^{12}	cm^{-2}
κ	0.01 to 10	dyn cm^{-1}
λ	1 to 4	10^{-6} cm
M_b	10^{-12} to 10^{-13}	ergs
B_z	4.1×10^{-14}	ergs

The estimate of the bending modulus is based on the measurements of Evans (1983); other estimates are adapted from the discussion of Bell *et al.* (1984). From the numbers listed above it can be concluded that the value of β is typically much less than one. Physically this means that the cell membrane is quite rigid compared with the bonds.

RESULTS

Figure 2 illustrates the time dependence of the peeling velocity in the case of slip-bonds. Computations corresponding to T_{fx} of twice the critical tension, T_{fx} equal to the critical tension and T_{fx} of half the critical tension are demonstrated. To show how the results depend on the choice of contact threshold, each computation was done for $\epsilon_c = 10^{-4}$ (open symbols) and for $\epsilon_c = 10^{-6}$ (closed symbols). In all

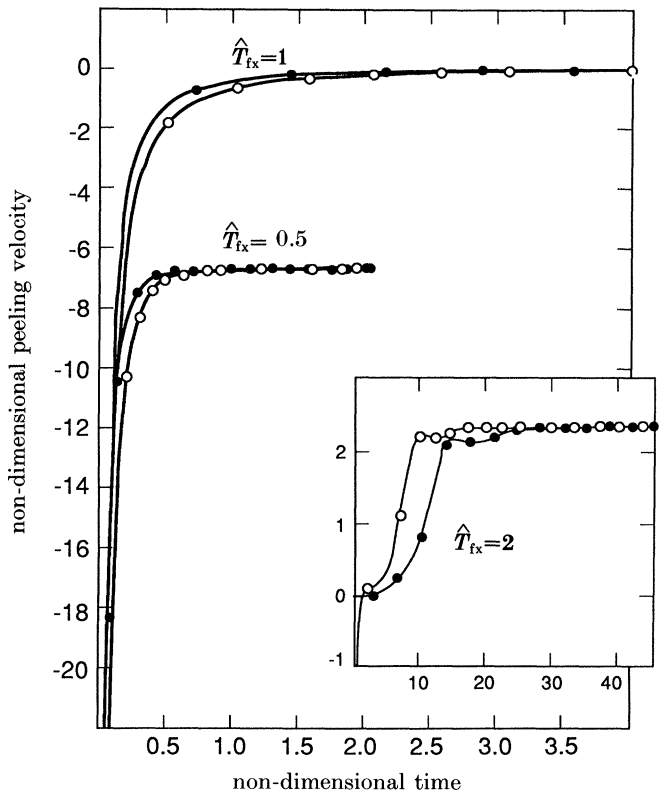

FIGURE 2. Six computations of the time dependence of the peeling velocity in the case of slip-bonds. In all cases the initial bond distribution is of the form given by (16). Three pairs of curves are shown corresponding to $\hat{T}_{fx} = 0.5$, 1.0 and 2.0. Within each pair the curve corresponding to non-dimensional contact threshold ($\epsilon_c = A_{b,c}/A_{b,eq}$) of 10^{-4} is marked by open symbols, and the curve for 10^{-6} by closed symbols. In all six computations $\beta = 1.68 \times 10^{-4}$, $\theta_{fx} = \frac{1}{2}\pi$, $K_{eq} = 1.0$, and $F_\kappa = 0.0$. In all cases a steady state of peeling is approached asymptotically at long times. Once this state is attained, the velocity does not depend on the choice of contact threshold.

cases, the existence of an initial transient phase during which the peeling velocity undergoes considerable excursions can be seen. During the transient phase, the peeling velocity depends slightly on the choice of contact threshold. However, as remarked earlier, the steady-state peeling velocity is independent of the choice of contact threshold.

Figure 3 shows the typical time dependence of peeling and annealing for the case of catch-bonds. To facilitate comparisons, the computations in figures 2 and 3 are matched in all respects except that in figure 3 $F_\kappa = -0.05$ whereas in figure 2 $F_\kappa = 0.0$. There are some small changes in the time-course of annealing and in the final steady-state annealing velocity; these are more or less linear in F_κ and will be discussed more fully later on. In contrast, the time-course of the peeling mode (shown in the insert of figure 3) is completely transformed. Most importantly, the steady-state peeling velocity in the insert of figure 3 is zero. This last result is a completely general property of catch-bonds; if bonds are of catch-type and if the

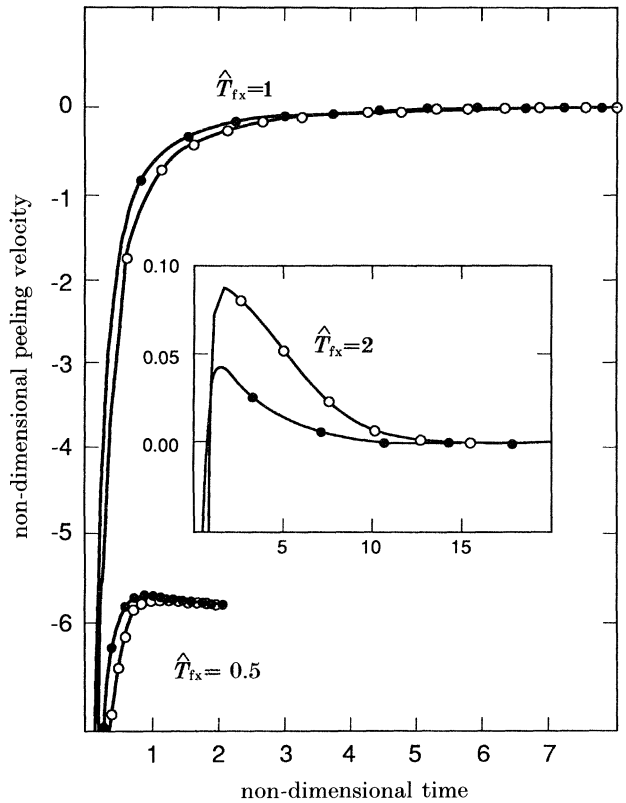

FIGURE 3. Six computations of the time dependence of peeling in the case of catch-bonds. The format description of figure 1 applies equally well to this figure. Parameter values are also the same as in figure 2, except that the value of $F_\kappa = -0.05$. In the case of catch-bonds, the steady-state peeling velocity always equals zero when the tension exceeds the critical tension. At tensions less than the critical tension there is little difference between slip-bonds and catch-bonds.

tension is greater than or equal to the critical tension, then, no matter how other parameters are chosen, the membrane will start to peel but will quickly grind to a halt. This behaviour is all the more remarkable when one considers that for tensions less than or equal to the critical tension, the behaviour of catch-bonds is very similar to that of slip-bonds. In other words, the equations governing the formation of catch-bonds seem to be (and in fact are) fully reversible in a thermodynamic sense. Nevertheless, although the membrane can anneal to a surface, it is impossible to peel it off again. The solution of this seeming paradox lies in the fact that bond formation is only reversible at thermal equilibrium when Maxwell's demon is asleep. When tension in excess of the critical tension is applied, the demon awakens.

Except to verify that steady states always occur after sufficient time, we have not made an extensive study of the detailed characteristics of the transient phase of peeling or annealing. Such a study might be very interesting, however, because in some cases we find that the early kinetics of peeling are remarkably complex

even in the case of slip-bonds. When K_{eq} is large, the kinetics of detachment consist of a long lag phase followed by abrupt acceleration and overshoot of the stable peeling rate and finally an approach to the stable rate through a sequence of damped oscillations. These phenomena are quite prominent in the computation shown in figure 4. The potential complexity and long duration of the lag phase of peeling should serve as a warning against overly facile assumptions in the interpretation of experimental results. For example, in measurements of the rate of detachment of adherent cells (Mohandas *et al.* 1974; Mege *et al.* 1986), it is possible that the results are completely dominated by the initial transient.

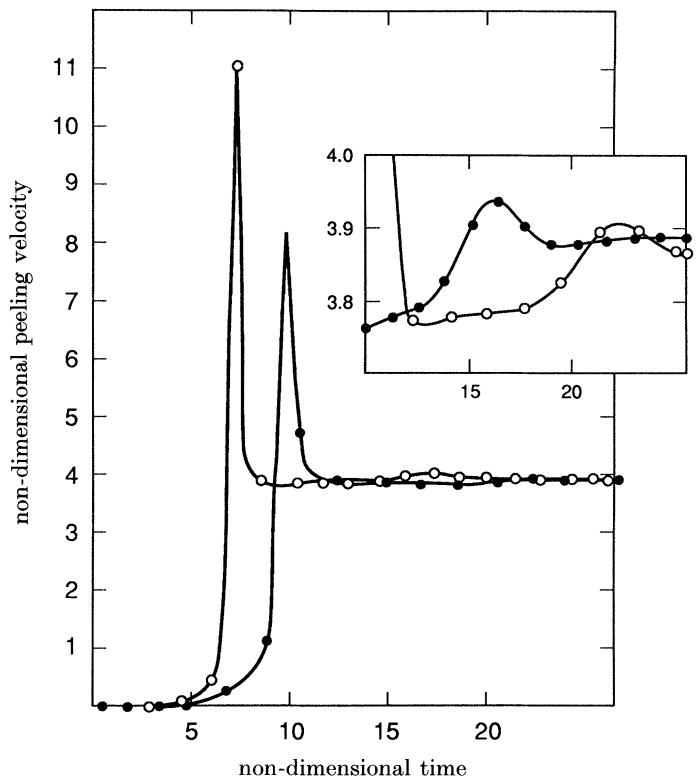

FIGURE 4. A computation illustrating the phenomena of lag-phase overshoot and damped oscillations in the kinetics of peeling. Parameter values: $\theta_{fx} = \frac{1}{2}\pi$; $\hat{T}_{fx} = 2.0$; $\beta = 1.68 \times 10^{-5}$; $K_{eq} = 100$; $F_\kappa = 0$. $\epsilon_c = 10^{-3}$ (open symbols) and 10^{-4} (closed symbols).

We now consider the geometric character of the steady-state solutions of our model. Figure 5*a–c* gives the steady-state solutions corresponding to the end points of the three kinetic computations shown in figure 2. Figure 5*a* represents a steady state of annealing, figure 5*b* shows the final state at the critical tension, and figure 5*c* corresponds to a steady-state of peeling. These are typical of the solutions obtained for all slip-bonds and also for catch-bonds if the tension is less than the critical tension. Figure 6 shows the nature of the steady state in the case of catch-bonds when the tension is greater than the critical tension. Parameter values for the computation in figure 6 are matched with those of figure 3.

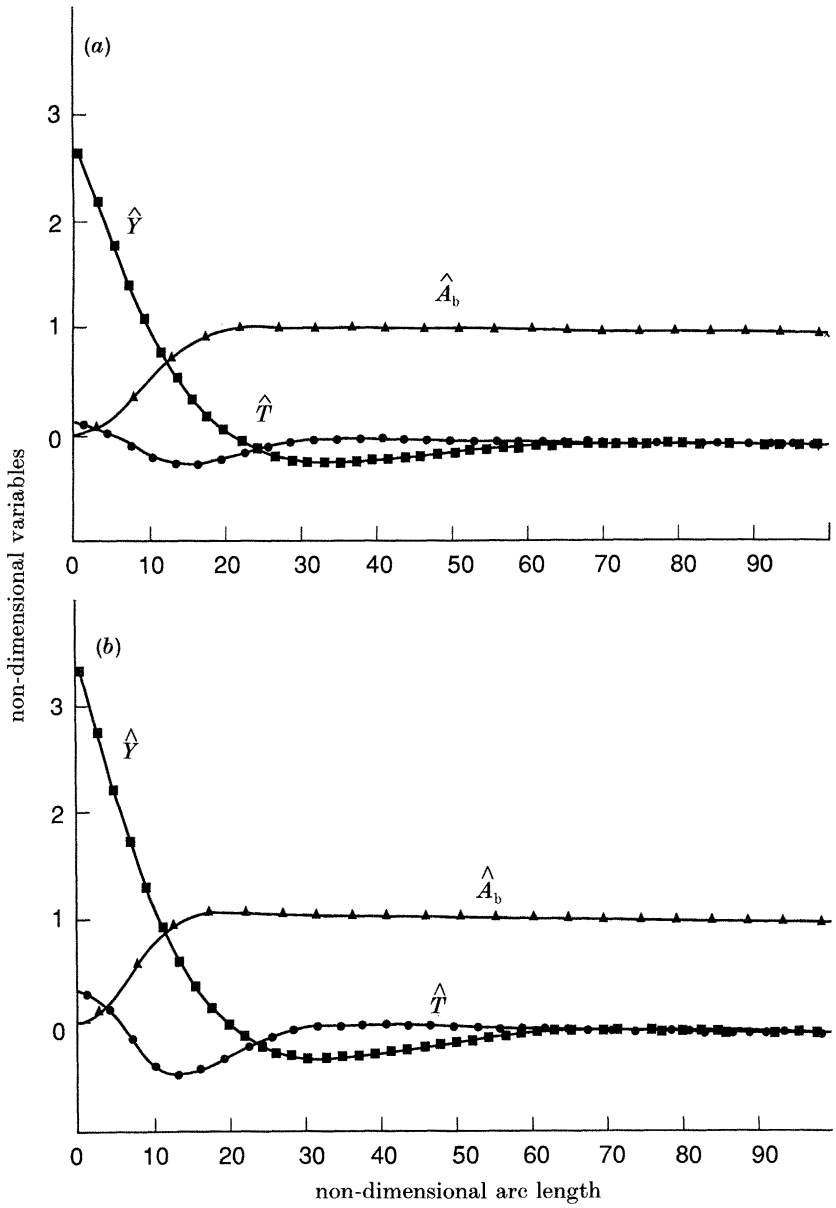

FIGURE 5(*a*, *b*). For description see opposite.

The horizontal axis in figures 5*a–c* and 6 corresponds to non-dimensional arc length ($\tilde{s}$). As a function of $\tilde{s}$, each figure gives the non-dimensional gap separating the membrane from the surface ($\hat{Y}$), the non-dimensional bond density ($\hat{A}_b$), and the non-dimensional tension ($\hat{T}$). For those who are unfamiliar with the physics of membrane bending, it is usually surprising to discover that $\hat{Y}$ undergoes damped oscillations. At first approach its finite bending stiffness causes the membrane to overshoot the equilibrium separation so that the bonds become compressed

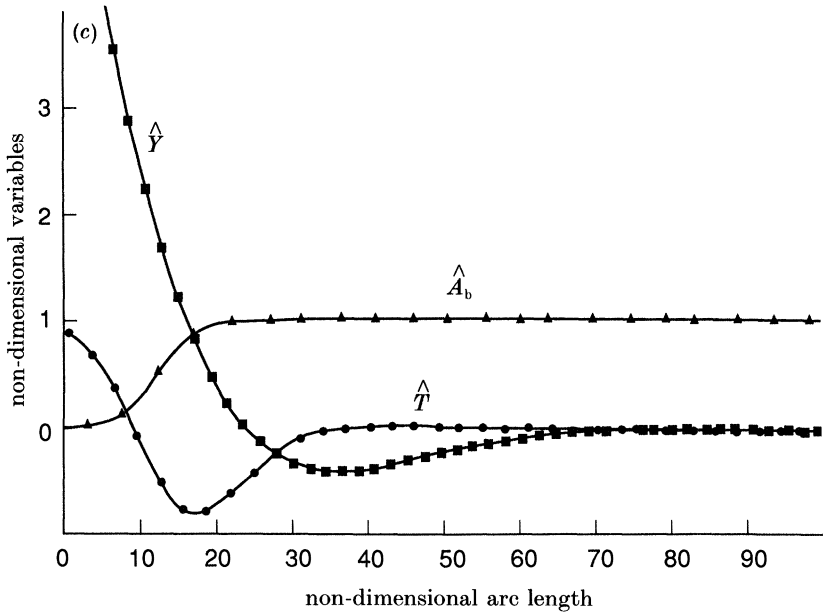

FIGURE 5. Spatial variation of $\hat{Y}$, $\hat{T}$, and $\hat{A}_b$ at steady state in the case of slip-bonds. Graphs (*a–c*) correspond to $\hat{T}_{fx} = 0.5$, 1, and 2, respectively. Other parameters are the same as in figure 2: $\theta_{fx} = \frac{1}{2}\pi$; $\beta = 1.68 \times 10^{-4}$; $K_{eq} = 1$ and $F_\kappa = 0$. See (29*a–h*) for definitions of non-dimensional quantities.

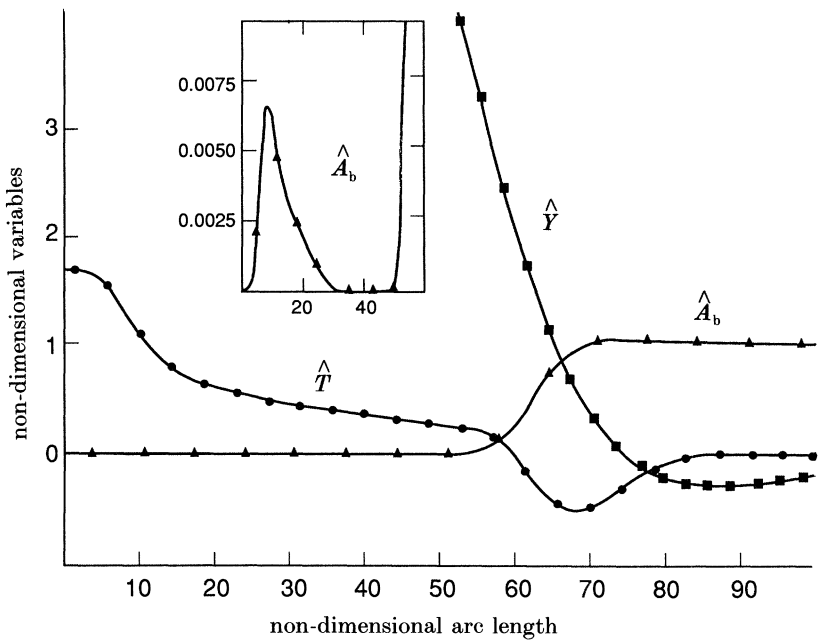

FIGURE 6. Spatial variation of $\hat{Y}$, $\hat{T}$, and $\hat{A}_b$ in the 'catch-state'. Parameter values are the same as in figure 3. The catch-state is caused by the presence of a few highly stretched bonds. The density and distribution of these bonds cannot be seen on the standard scale but can be demonstrated on the expanded scale of the insert. These few bonds by themselves must counterbalance most of the tension applied to the membrane.

($\hat{Y} < 0$). The upward force of the bonds eventually causes the trajectory of the membrane to turn upwards. Once again the equilibrium separation is overshot causing the bonds to stretch, and so forth. At each cycle the amplitude of undershoot or overshoot diminishes exponentially until the final equilibrium separation is attained. Unfortunately, in figure 5*a–c*, only the first cycle is of sufficient amplitude to be visible; nevertheless, the principle is clear.

If $\hat{V}_{\rm pl}$ is very close to zero, then, according to (22) and (24), the spatial dependence of the tension and bond density are simply related to the variations of $\hat{Y}$. Equations (24) and (26) hold exactly for the computation in figure 5*b*. Unfortunately, the comparison with the results shown in figure 5*a*, *c* demonstrates that the expansion of the bond density in powers of the velocity (21) is very slowly converging. Thus, although one can obtain an approximate expression for the peeling velocity by neglecting all but a few terms of the power series, the result is not very useful in itself. Nevertheless, the result does serve as a point of departure for the empirical analysis of numerical computations (see (34)).

During the process of peeling the spatial variations of the bond density are translated into temporal variations of the peeling rate by the effects of virtual convection. This connection explains the complex kinetics seen in figures 2 and 4, and is really quite trivial once it is pointed out.

The spatial variations of $\hat{A}_{\rm b}$, $\hat{Y}$ and $\hat{T}$ for the case of catch-bonds reveal the essence of why such bonds act the way they do. As shown by the insert in figure 6, there is a secondary accumulation of bonds with maximum density at $\tilde{s}$ approximately equal to 10. There are not very many bonds at this location; in fact the whole phenomenon is not even directly visible on the scale of the main plot. Nevertheless, these few bonds are important because they are under extremely high strain ($\hat{Y} = 28$–29 at $\tilde{s} = 10$). The tangential traction they exerted is responsible for the sudden decline in the tension between $\tilde{s} = 10$ and $\tilde{s} = 30$. This traction counteracts the brunt of the applied tension, bringing the effective tension acting on the remainder of the membrane down to the level of the critical tension. Obviously, the situation shown in figure 6 is not in thermal equilibrium; however, we emphasize that the system is in mechanical equilibrium. In fact, if we take the lifetime of an unstrained bond to be about 1 ns, then it can readily be estimated from (19) that the lifetime of one of the highly stretched catch-bonds at $\tilde{s} = 10$ exceeds the current age of the universe by a comfortable margin.

We now turn to the main object of our study: the steady-state peeling velocity. We have already seen that this object is trivial in the case of catch-bonds when the tension exceeds or equals the critical tension; to wit, $\hat{V}_{\rm pl} = 0$ regardless of other parameters. In the remaining situations we are unable to provide an exact expression for the peeling velocity. Fortunately, this is not a significant drawback because we have been able to discover an extremely accurate and general asymptotic formula only involving simple analytic combinations of the fundamental non-dimensional parameters.

To write the expression for the peeling velocity we first define the three quantities:

$$Q_1 = 2\pi[\{-b+[c+b^2]^{\frac{1}{2}}\}^{\frac{1}{2}}], \tag{31}$$

where $$b = \frac{[\beta(1+K_{eq})\ln(1+K_{eq})\hat{T}_{fx}]}{[(1+1.5K_{eq})(1+\cos(\theta_{fx}))]}$$

and $$c = [0.5\beta K_{eq}]/[(1+2K_{eq})];$$

$$Q_2 = 1+\hat{T}_{fx}^{-1}+(K_{eq}/(1+K_{eq}))\hat{T}_{fx}^{-d}, \tag{32}$$

where $$d = [(1+K_{eq})\ln(1+K_{eq})]/K_{eq};$$

and $$Q_3 = 1+2dF_\kappa\hat{T}_{fx}+O[(F_\kappa\hat{T}_{fx})^2]. \tag{33}$$

In terms of these quantities, the approximate expression for the steady-state peeling velocity is simply

$$\hat{V}_{pl} = Q_2 Q_3 \ln(\hat{T}_{fx})/Q_1. \tag{34}$$

To assess the accuracy of (34), we ran a program of approximately 600 computations designed to cover broadly the combinatorial choices of non-dimensional parameters falling within the physically reasonable range. θ_{fx} was between 0 and $\frac{7}{8}\pi$, $\hat{T}_{fx}$ was between 0.5 and 8, β was between 10^{-6} and 2×10^{-2}, K_{eq} was between 10^{-3} and 10^{+3}, and F_κ was between 0 and 0.05. In this series of tests the average percentage difference between the prediction of (34) and the numerical result was 10.7%. There were 15 computations in which the error exceeded 20% and no cases in which the error exceeded 30%. Of the 15 cases in which the error exceeded 20%, all involved computations in which K_{eq} was greater than 10; otherwise no systematic factor associated with high error could be determined.

It would be good if we were able to give some rigorous mathematical explanation for the extraordinary accuracy and generality of (34). Unfortunately, such an explanation is unknown, at least to us. The derivation of (34) was accomplished by an *ad hoc* combination of guesswork, knowledge of limiting cases, some facility with jigsaw puzzles, scaling arguments, and careful study of a very large number of numerical calculations. Those who are uncomfortable with such an essentially experimental approach to applied mathematics are sincerely encouraged to attempt a more systematic derivation.

Figure 7 illustrates the dependence of $\hat{V}_{pl}$ on $\hat{T}_{fx}$ and K_{eq} for the case when β is very small, F_κ is zero and $\theta_{fx} = \frac{1}{2}\pi$. Symbols are used to represent the numerical results; whereas the smooth curves give the predictions of (34).

Under the circumstances of the computations shown in figure 7, $Q_3 = 1$ and the coefficient Q_1 approaches a constant independent of tension (see (31)). Qualitatively, $\hat{V}_{pl}$ has a strong singularity as $\hat{T}_{fx}\to0$ because of the influence of the coefficient Q_2. As the value of K_{eq} gets large, the exponent of this singularity approaches infinity because of the term $\hat{T}_{fx}^{-d}$ (see (32)). For non-dimensional tensions greater than one, Q_2 rapidly approaches one, and thereafter $\hat{V}_{pl}$ increases logarithmically with the tension. When K_{eq} is large, there is a small systematic difference between the numerical computation of $\hat{V}_{pl}$ and the values computed by using (34). This sort of phenomenon accounts for almost all the discrepancy between (34) and the numerical results. The example shown is the worst case of such discrepancy. Of the 15 instances in which the error of (34) exceeds 20%, eight can be found in figure 7.

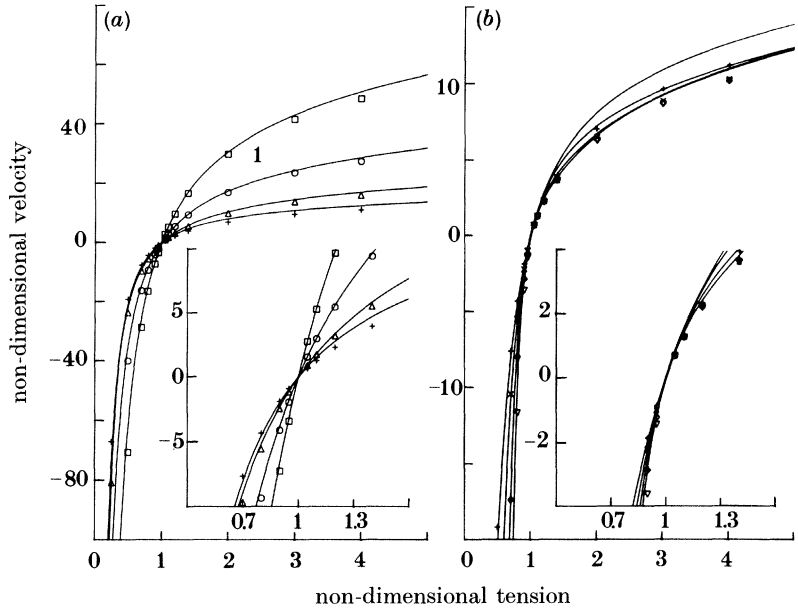

FIGURE 7. Dependence of $\hat{V}_{\rm pl}$ on $\hat{T}_{\rm fx}$ for various values of $K_{\rm eq}$. Fixed-parameter values are: $\beta = 1.68 \times 10^{-6}$, $\theta_{\rm fx} = \frac{1}{2}\pi$ and $F_\kappa = 0$. (*a*) Results from numerical calculations for $K_{\rm eq} = 0.001$ (squares), $K_{\rm eq} = 0.01$ (circles), $K_{\rm eq} = 0.1$ (triangles) and $K_{\rm eq} = 1.0$ (plus signs). (*b*) Results for $K_{\rm eq} = 1.0$ and numerical results for $K_{\rm eq} = 10$ (crosses), $K_{\rm eq} = 100$ (diamonds) and $K_{\rm eq} = 1000$ (inverted triangles). The smooth curves are drawn by using (34).

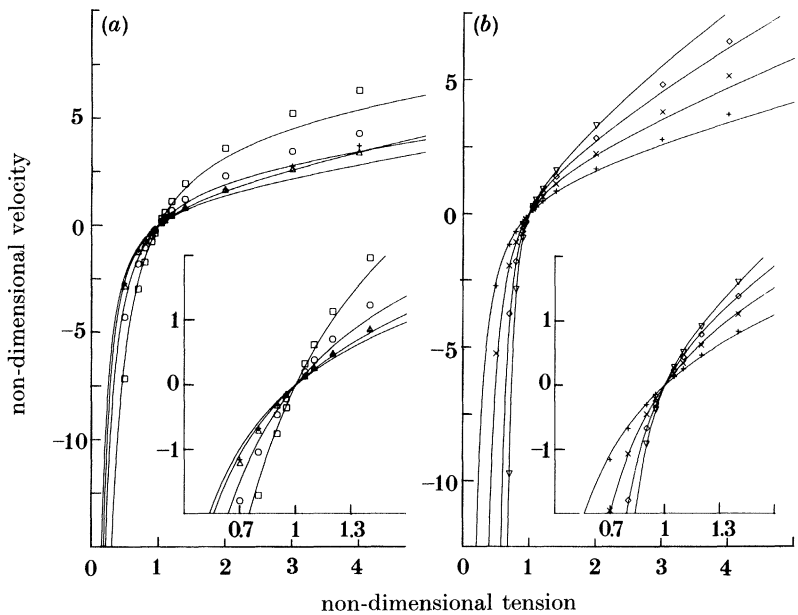

FIGURE 8. Dependence of $\hat{V}_{\rm pl}$ on $\hat{T}_{\rm fx}$ for various values of $K_{\rm eq}$. Fixed-parameter values are: $\beta = 1.68 \times 10^{-2}$, $\theta_{\rm fx} = \frac{4}{5}\pi$ and $F_\kappa = 0$. The numerical results (indicated by symbols) and the comparison to (34) (smooth curves) are organized according to the same format as in figure 7.

Figure 8 shows a series of computations in which F_κ is still equal to zero, but in which the other parameters have been changed so as to magnify the nonlinear tension dependence of Q_1. As before, agreement between the computations and (34) is excellent.

Figure 9 illustrates the results obtained if $F_\kappa > 0$. The main consequence of taking $F_\kappa > 0$ is that $\hat{V}_{\rm pl}$ now increases at a faster than linear rate when the tension is large.

Thus (34) is useful because it expresses the predictions of our model in a compact and accessible form.

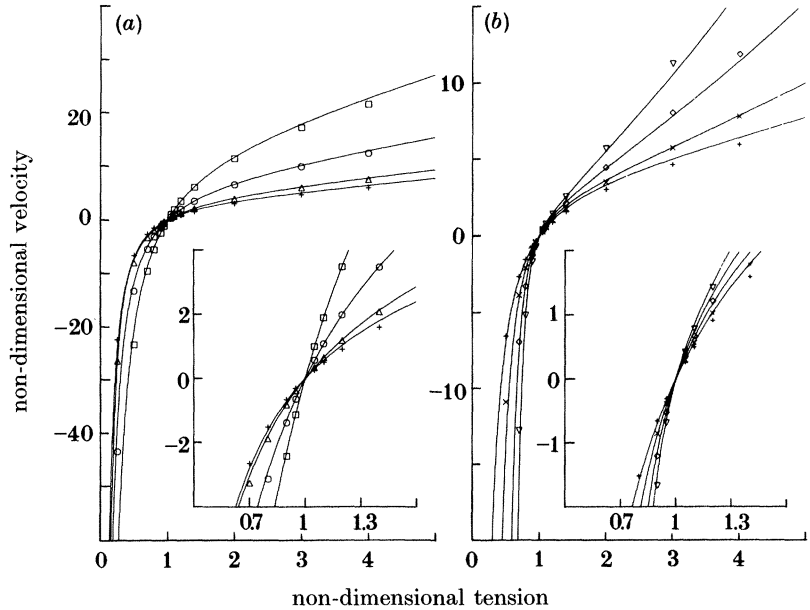

FIGURE 9. Dependence of $\hat{V}_{\rm pl}$ on $\hat{T}_{\rm fx}$ for various values of $K_{\rm eq}$. Fixed-parameter values are: $\beta = 1.68 \times 10^{-4}$, $\theta = \frac{1}{2}\pi$, and $F_\kappa = 0.05$. The numerical results (indicated by symbols) and the comparison with (34) (smooth curves) are organized according to the same format as in figure 7.

ANALYSIS OF EXPERIMENT

As an application of (34) we will reanalyse some results of a well-known study of the motion and adhesion of granulocytes in the postcapillary venules of mouse mesentery and hamster cheek pouch (Atherton & Born 1972, 1973). In that study it was shown that granulocytes adhere to the vascular endothelium while rolling due to the shear force of the flowing blood. Thus new adhesive bonds must form at the front of the cell, and membrane is peeled from the surface at the trailing edge of the cell.

To apply our model to the Atherton–Born study, we must make a mapping between the problem of a cell that rolls because hydrodynamic shear acts on its upper surface, and the problem of a tape that peels because tension is applied to its free extremity. Implicit in such a mapping is the assumption that the dominant factor resisting forward motion of the rolling cell is the breaking of adhesive bonds. Thus we propose that the important dissipation of energy in a rolling cell occurs in a very localized region at the trailing edge.

Because the surface of the granulocyte has many small folds, or is 'wrinkled', the localized region of peeling should probably be thought of as corresponding to a single such 'wrinkle'. With this in mind, we shall take advantage of the fact that on a molecular-distance scale (i.e. from the point of view of the bonds) the distinction between rolling and peeling becomes rather academic. Thus we can loosely think of the bonds under the main body of the cell as mechanically equivalent to the clamp, and the fluid flowing over the free surface of the cell as generating an applied tension.

It is known that the blood undergoes Poiseuille flow through the venules. If we assume that the membrane is slack in the absence of blood flow, then one can estimate without too much difficulty that

$$T_{\mathrm{fx}} \approx 8 D_{\mathrm{gran}} V_{\mathrm{blood}} \eta_{\mathrm{blood}} / D_{\mathrm{venule}}, \tag{35}$$

where V_{blood} is the mean flow velocity of the blood, η_{blood} is the viscosity of the blood, D_{venule} is the diameter of the venule, and D_{gran} is the diameter of the granulocyte.

We can also assume that the value of β for the granulocyte is much less than one (see section on information structure for justification). In this case the value of θ_{fx} need not be accurately estimated because it has a negligible effect on the peeling velocity.

The main point of (35) is that the effective tension at the free extremity in the equivalent peeling problem is proportional to the mean velocity of the blood. In addition, the constant of proportionality is a simple function of various known quantities. This means that one can quantitatively observe the effects of varying the tension because blood velocity varies naturally from venule to venule over a large range. V_{blood} and hence T_{fx}, can also be controlled by constricting an arterole serving the venule being observed.

Figure 10 shows the correlation between the velocity of rolling granulocytes and the velocity of the blood according to Atherton & Born. Each data point represents the average over many granulocytes passing a fixed observation point in a single vessel of the mouse mesentary preparation. Thus the scatter of the data points is due to random differences in the properties of the vessels, not to errors of measurement.

It is apparent from figure 10 that the granulocyte velocity intersects the horizontal axis as the blood velocity approaches a certain critical value. The existence of such a critical velocity is certainly a necessary prediction of our model.

Because T_{fx} is proportional to V_{blood}, we can express the non-dimensional tension in terms of the blood velocity. If we cast out those terms that are negligible at small β and at large T_{fx}, then (34) predicts that the dependence of the granulocyte velocity on the mean blood velocity will be of the form

$$V_{\mathrm{gran}} \approx p_1 (1 + p_0 / V_{\mathrm{blood}}) (1 + p_2 V_{\mathrm{blood}} / p_0) \ln (V_{\mathrm{blood}} / p_0), \tag{36}$$

where

$$p_0 = T_{\mathrm{crit}} D_{\mathrm{venule}} / (8 \eta_{\mathrm{blood}} D_{\mathrm{gran}}),$$

$$p_1 = K_{\mathrm{r}}(\lambda) (B_z / \kappa)^{\frac{1}{2}} / [2\pi \{0.5 \beta K_{\mathrm{eq}} / (1 + 2K_{\mathrm{eq}})\}^{\frac{1}{4}}]$$

and

$$p_2 = 2F_\kappa (1 + K_{\mathrm{eq}}) \ln (1 + K_{\mathrm{eq}}) / K_{\mathrm{eq}}.$$

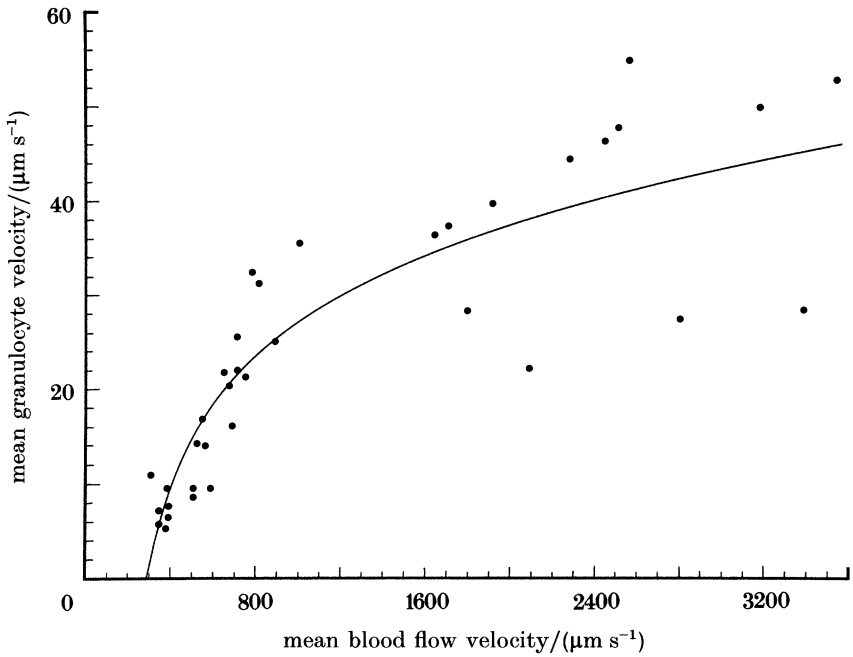

FIGURE 10. Comparison between the model and the data of Atherton & Born (1973). Data points represent the average velocity of granulocyte rolling and average velocity of blood flow in 36 individual venules of the mouse mesentery. The smooth curve represents the least squares fit of the expression for V_{gran} (i.e. (36)). The parameter values determined by the nonlinear least squares procedure are discussed in the text.

The smooth curve in figure 10 shows the best fit of (36) to the data of Atherton & Born. The maximum likelihood values of the parameters together with estimated 90% confidence intervals are:

$$p_0 = 295\ \mu\text{m s}^{-1} \quad (232 \text{ to } 323)$$

$$p_1 = 18\ \mu\text{m s}^{-1} \quad (11 \text{ to } 18)$$

$$p_2 = 0 \quad (0 \text{ to } 4.6 \times 10^2)$$

Because the fit shown in figure 10 is excellent, we conclude that our model is at least consistent with the highly nonlinear correlation between V_{gran} and V_{blood} discovered by Atherton & Born. This is not a trivial result. For example, because they study a Newtonian adhesive, McEwan & Taylor obtain a linear relation between tension and peeling velocity at large velocities. At the other extreme, if one proposes that bonds experience elastic deformation until a critical failure stress is reached (see, for example, Evans 1985*a*), then the peeling velocity is infinite (or at least undefined) except at the critical tension. It seems that to obtain a realistic tension–velocity relation it is necessary to propose some ability of the adhesion molecules to store elastic potential energy, but failure of the bonds cannot be viewed as a deterministic event.

From the value of p_1, we calculate that the critical tension for adhesion between

a granulocyte and the vascular endothelium is about 2×10^{-3} dyn cm^{-1}†. This is a perfectly reasonable value for the critical tension of a biological adhesion; similar critical tensions (5×10^{-5} to 5×10^{-3}) were obtained by Mohandas *et al.* (1974) in the case of red-cell adhesion to various surfaces. Evans & Buxbaum (1981) obtained values of between 7×10^{-4} and 7×10^{-2} dyn cm^{-1} in the case of dextran-mediated adhesion of red cells to particles.

Examination of the expression for the lumped parameter p_2 shows that this quantity must be at least two times larger than the value of F_κ. Thus the fact that the data can only be explained if p_2 is close to zero means that we can reject any proposal in which F_κ is significantly greater than 2%. This is certainly consistent with the physical interpretation of F_κ.

The parameter p_1 is a complex function of all the physical constants of the model, and its value though interesting in itself does not yield a strong test of physical consistency.

Let us next consider the experimental evidence for the existence of the peculiar theoretical constructs that we call catch-bonds. Fortunately, the existence of catch-bonds should be fairly easy to recognize. If adhesion is mediated by catch-bonds, then, no matter how much tension is applied, it is impossible to achieve significant separation of the surface and the membrane short of doing irreversible damage. This is not because catch-bonds are necessarily 'strong' or energetically favourable in some sense. For example, catch-bonds could have very low critical tension and very low value of the forward rate constant. Thus one can have the paradox of two surfaces which have little or no spontaneous tendency to adhere but which are impossible to separate if forced into contact.

Findings that have an uncanny resemblance to what one expects for catch-bonds have been reported (Evans & Leung 1984) in a study of red-cell adhesion mediated by wheatgerm agglutinin. These authors found that, despite a low critical tension for spontaneous adhesion, it required very great tension to separate the cells. Also, when separation did occur, reattachment was not possible. The irreversibility of separation was shown to be due to lateral pulling of the adhesion molecules through the plane of the membrane.

Evans (1985*b*) has reanalysed these data and has quite forcefully pointed out the paradoxical nature of the evidence when analysed by conventional models. In this reanalysis, Evans attributes the seeming paradoxes to a discrete or discontinuous distribution of adhesion molecules. It seems that both this approach and the approach based on catch-bonds are consistent with the available data and that further experiments would be useful.

We find it impossible to resist some speculative remarks concerning the physiological significance of these putative catch-bonds. It is well known that the specialized adductor muscle of molluscs is able to lock when contracted and then maintain tension without any more consumption of metabolic energy. The tension can be maintained for a very long time: until a release signal is received. This behaviour certainly supports the general idea of catch-bonds. It would also suggest that the actin–myosin crossbridges of the adductor muscle can convert from

† 1 dyn = 10^{-5} N.

catch-bonds to slip-bonds in response to some regulatory factor. Is it possible that such regulation could also occur in the context of cell adhesion? Could such a regulatory effect be responsible for what is frequently described as the 'slow energy-dependent strengthening' of adhesion?

Recently, the structure of neural cell adhesion molecules (NCAM) has been elucidated at low resolution (Hall & Rutishauser 1987). It was shown that the molecule has a distinct 'hinge' region. This is interesting for our understanding of catch-bonds and slip-bonds. We would predict that if NCAM form catch-bonds then this hinge will be stiff before bonding and will undergo a conformational relaxation during bond formation. If NCAM form slip-bonds, then the hinge will be most flexible in the non-bonded state and will stiffen during binding.

Experiments in non-biological systems have long shown that for many adhesives the process of tape peeling does not always attain a steady state. Particularly if the tensions are very large, the asymptotic behaviour corresponds to sustained yield–stick oscillations of very large magnitude and highly nonlinear wave form (these experiments are reviewed by Krenceski *et al.* (1986)). When these oscillations are of high frequency, they are responsible for the 'tearing' sound that one sometimes hears when pulling adhesive tape from a roll.

Given these remarkable experimental facts, it was natural for us to make an exhaustive numerical search for the existence of stable oscillatory solutions of our model. Despite this search, we were unable to discover stable oscillations, although damped oscillations were observed (see Results). It is still possible that sustained oscillations exist in some narrow or inaccessible region of parameter space, but this is very doubtful. The essential conclusion we draw is that our model cannot explain the existence of oscillatory peeling modes.

Sung *et al.* (1985*a*, *b*) have reported some interesting measurements of the critical tension of erythrocyte aggregation induced by two different *N*-acetyl-galactosamine reactive lectins. These are *Helix pomatia* agglutinin (HPA) and *Dolichos biflorus* agglutinin (DBA). By using the flow-channel technique developed by Chien, it was found that the shear stress at 50% separation of doublets of RBCs was proportional to the surface density of lectin. This is in accord with the prediction of (26).

For both lectins, the ratio of surface energy to surface density was found to be between 0.25 and 0.30×10^{-4} ergs per molecule†. Because the contact angle in the channel flow technique is close to zero, we conclude from (24) that for both HPA and DBA, the value of K_{eq} is approximately equal to 0.1. This must be regarded as a lower bound on K_{eq} because we have implicitly assumed that all lectin molecules bound to the surface are available to form crossbridges, and we have also neglected the non-specific repulsive potential.

An additional *caveat* in interpreting the studies of Sung *et al.* (1985*a*, *b*) comes from the fact that the reversibility of the peeling process was not studied. Thus it is possible that irreversible damage was being done to the cells in a fashion analogous to the situation found with wheatgerm agglutinin (see above).

To see if the value of $K_{eq} = 0.1$ is a reasonable lower bound, one can examine

† 1 erg = 10^{-7} J.

independent data on the adsorption of these lectins to the cell surface directly from the solution. Unfortunately, a measurement of the adsorption constant is not available for HPA. In the case of DBA the value of the adsorption constant to the red-cell surface was found to be

$$K_{\text{adsorp}} = (\text{equilibrium surface density})/(\text{equilibrium concentration in solution}) = 0.9 \times 10^{-4} \text{ cm}.$$

To convert between K_{adsorp} and K_{eq}, one must divide the former quantity by the characteristic amplitude of the thermal vibrations of the position of a lectin molecule bound to a cell-surface carbohydrate. This amplitude should certainly be more than 1 Å† and less than 100 Å. Therefore we conclude that on the basis of the measured adsorption constant the value of K_{eq} should be about 1000 instead of 0.1.

A discrepancy of a factor of 10^4 can hardly be called satisfactory agreement. Nevertheless, the size of the discrepancy is somewhat exaggerated because K_{eq} appears in the logarithm. Thus the discrepancy could be resolved if one were to assume that only 1% of bound lectin was available for crossbridging. These considerations serve mainly to illustrate the frustrations of testing quantitative theories in this area.

Conclusion

The model we have discussed makes three major assumptions that are rather tenuous and that ultimately limit its utility. These are: (*a*) that the bonding stresses are the only distributed stresses acting on the membrane; (*b*) that the bonds are fixed in the plane of the membrane; and (*c*) that the chemical reaction of bond formation and breakage is reversible. Lest the gullible be too easily taken in by the seeming rationality of our presentation, we shall dwell somewhat on the seriousness of the problems raised by these assumptions.

In addition to bonding stresses, real biological membranes experience stresses due to the force fields exerted by surrounding objects, due to gradients of hydrostatic pressure across the membrane, due to contractile filaments inside the cell, due to elastic skeletal elements inside the cell, and also due to hydrodynamic pressures and viscous shears caused by motion of the membrane relative to the surrounding fluid.

Major leverage in the theoretical treatment of these complex forces comes from the fact that in some cases they operate on a distance scale that is very different from the scale involved in bonding. This allows separation of the problem into 'inner' and 'outer' regions in the fashion of boundary-layer theory. In a simplified and non-rigorous way this is what we have done in our treatment of the Atherton–Born study (see preceding section). This approach cannot be successful in the case of short-range forces between the membrane and the surface. Much work remains to be done on the treatment of the latter.

It is known that adhesion molecules are frequently able to diffuse laterally in the plane on the membrane. If this is the case, then the process of adhesion and

† 1 Å = 10^{-10} m = 10^{-1} nm.

detachment cannot be dominated solely by events in a localized contact zone. Global redistribution and recruitment of adhesion molecules into the contact region becomes important. Such processes can lead to large effects at thermal equilibrium (see Bell *et al.* 1984), and it is to be expected that they will also have large effects on the kinetics of adhesion. In any event if diffusion of adhesion molecules is important, then the model we have presented is not applicable.

An additional problem related to lateral mobility of adhesion molecules is raised by the data of Evans & Leung (1984) concerning separation of red cells held together by wheatgerm agglutinin (see preceding section). It is apparent from these studies that even if lateral redistribution of adhesion molecules is normally negligible, this need not remain the case once tension is applied to the membrane. Our computations show that the adhesion molecules at the edge of the contact zone experience very large shear stresses, especially in the catch state. Thus it is not surprising that they can be torn loose from their moorings and accumulated into the contact region.

The final *caveat* concerns the implications of our assumption of reversible binding. This assumption implies that there is only one chemical pathway by which bonds can break when tension is applied and also that the result of bond breakage is always to regenerate a functional adhesion molecule. Obviously this is a very idealized and dangerous proposition.

From the above catalogue of woes it would seem that there is a long way to go in developing a quantitative understanding of biological adhesion. We hope that the results we have presented will stimulate interest in the use of peel analysis as a tool for furthering such understanding.

Appendix 1

The results discussed in the main body of the text relate to a particular form of the constitutive law connecting bond strain to reaction rate. This form arises from the assumption that the difference between the transition-state spring and the final bound-state spring occurs only in the spring constant and not in the rest length (see discussion leading to (16)). This assumption is plausible and leads to simple results, but it is not in any sense a necessary truth.

Suppose that we now make the opposite assumption; i.e. suppose that the spring constant of the transition state is the same as in the bound state but that the rest lengths of the two forms of the adhesion molecule are slightly different. If this is the case, then instead of (18) and (19) we obtain the following constitutive laws:

$$K_f(Y) = K_f(\lambda)\exp\{-0.5\kappa((Y-\lambda)^2)/B_z\}\exp\{\kappa(\lambda_{ts}-\lambda)(Y-\lambda)/B_z\} \quad (A\ 1)$$

and

$$K_r(Y) = K_r(\lambda)\exp\{\kappa(\lambda_{ts}-\lambda)(Y-\lambda)/B_z\}, \quad (A\ 2)$$

where λ_{ts} is the rest length of the transition state.

It can be seen from (A 2) that if the transition state is shorter than the bound state then $K_r(Y)\to 0$ as $Y\to+\infty$. Thus, just as in the case of the standard constitutive law, one obtains a natural distinction between catch-bonds and slip-bonds. This is not simply a matter of formal mathematical definition; direct

computations show that the qualitative consequences of the catch-bond and slip-bond distinction are also insensitive to the detailed constitutive assumption.

The effects of a change in constitutive law is most readily gauged by the quantitative impact on the steady-state peeling velocity of slip-bonds. If one uses the expressions (A 1) and (A 2) instead of (18) and (19), we find that the basic form of (34) and the expressions for the coefficients Q_1 and Q_2 are unchanged. The expression for Q_3 becomes:

$$Q_3 = 1+2F_\lambda+2(F_\lambda^2(2d-1)T_{\hat{\mathrm{fx}}}), \tag{A 3}$$

where d is the same as in (32) and

$$F_\lambda = (\lambda_{\mathrm{ts}}-\lambda)(\kappa/B_{\mathrm{z}})^{\frac{1}{2}} \tag{A 4}$$

is a new non-dimensional parameter that takes the role previously played by F_κ. Note that bonds are slip-type only if $F_\lambda \geqslant 0$.

We conclude that the results we have described in the main text do not depend critically on the assumption that $\lambda_{\mathrm{ts}} = \lambda$.

Appendix 2

Glossary of symbols

$A_{\mathrm{b,c}}$	value of A_{b} at contact point
$A_{\mathrm{total}}, A_{\mathrm{f}}, A_{\mathrm{b}}$	total, free and bound surface densities of adhesion molecules
$A_{\mathrm{b,eq}}$	value of A_{b} at thermal equilibrium
B_{z}	product of Boltzmann's constant and absolute temperature
C	curvature
K_{eq}	equilibrium constant for formation of unstressed bonds
$K_{\mathrm{f}}(Y), K_{\mathrm{r}}(Y)$	forward and reverse rate functions
M_{b}	modulus of bending of membrane
P_{c}	arc length at contact point in laboratory frame
s	arc length in laboratory frame
$\tilde{s}$	arc length in contact point frame
t	time
T	tension
T_{crit}	critical tension
T_{fx}	tension at free extremity
X, Y	Cartesian coordinates
θ_{fx}	angle between membrane and surface at free extremity
$\kappa, \kappa_{\mathrm{ts}}$	spring constants of adhesion molecules in bonded state and transition state
$\lambda, \lambda_{\mathrm{ts}}$	rest length of adhesion molecules in bonded state and transition state
$\sigma_{\mathrm{tan}}, \sigma_{\mathrm{nor}}$	normal and tangential components of bonding stress

Various non-dimensional quantities ($\hat{A}_{\mathrm{b}}, \hat{A}_{\mathrm{f}}, \hat{t}, \hat{s}, B, F_\kappa, \epsilon_{\mathrm{c}}$, etc.) are defined in (28), (29) and (30). Three other useful non-dimensional quantities, b, c and d, are defined in (31) and (32).

References

Adamson, A. W. 1976 *Physical chemistry of surfaces.* New York: John Wiley & Sons.

Atherton, A. & Born, G. V. R. 1972 Quantitative investigations of the adhesiveness of circulating polymorphonuclear leucocytes to blood vessel walls. *J. Physiol., Lond.* **222**, 447–474.

Atherton, A. & Born, G. V. R. 1973 Relationship between the velocity of rolling granulocytes and that of the blood flow in venules. *J. Physiol., Lond.* **233**, 157–165.

Bell, G. I., Dembo, M. & Bongrand, P. 1984 Cell adhesion: competition between nonspecific repulsion and specific bonding. *Biophys. J.* **45**, 1051–1064.

Bongrand, P. & Bell, G. I. 1984 Cell–cell adhesion: parameters and possible mechanisms. In *Cell surface dynamics: concepts and models* (ed. A. S. Perelson, C. DeLisi and F. W. Wiegel), pp. 459–493. New York: Marcel Dekker.

Crocombe, A. D. & Adams, R. D. 1981 Peel analysis using the finite element method. *J. Adhesion* **12**, 127–139.

Crocombe, A. D. & Adams, R. D. 1982 An elasto-plastic investigation of the peel test. *J. Adhesion* **13**, 241–267.

Dembo, M. & Bell, G. I. 1987 The thermodynamics of cell adhesion. *Curr. Topics Mem. Trans.* **29**, 71–89.

Evans, E. A. 1983 Bending elastic modulus of red cell membrane derived from buckling instability in micropipet aspiration tests. *Biophys. J.* **43**, 27–30.

Evans, E. A. 1985*a* Detailed mechanics of membrane–membrane adhesion and separation. I. Continuum of molecular cross-bridges. *Biophys. J.* **48**, 175–183.

Evans, E. A. 1985*b* Detailed mechanics of membrane–membrane adhesion and separation. II. Discrete kinetically trapped molecular cross-bridges. *Biophys. J.* **48**, 185–192.

Evans, E. A. & Buxbaum, K. 1981 Affinity of red blood cell membrane for particle surfaces measured by the extent of particle encapsulation. *Biophys. J.* **34**, 1–12.

Evans, E. A. & Leung, A. 1984 Adhesivity and rigidity of erythrocyte membrane in relation to wheat germ agglutinin binding. *J. Cell Biol.* **98**, 1201–1208.

Evans, E. A. & Skalak, R. 1980 *Mechanics and thermodynamics of biomembranes.* Boca Raton, Florida: CRC Press.

Hall, A. K. & Rutishauser, U. 1987 Visualization of neural cell adhesion molecule by electron microscopy. *J. Cell Biol.* **104**, 1579–1586.

Krenceski, M. A., Johnson, J. F. & Temin, S. C. 1986 Chemical and physical factors affecting performance of pressure-sensitive adhesives. *J. Mater. Sci. Rev. macromolec. Chem. Physics* C**26**, 143–182.

McEwan, A. D. & Taylor, G. I. 1966 The peeling of a flexible strip attached by a viscous adhesive. *J. Fluid Mech.* **26**, 1–15.

Mege, J. L., Capo, C., Benoliel, A. M. & Bongrand, P. 1986 Determination of binding strength and kinetics of binding initiation. *Cell Biophys.* **8**, 141–160.

Mohandas, N., Hochmuth, R. M. & Spaeth, E. E. 1974 Adhesion of red cells to foreign surfaces in the presence of flow. *J. biomed. mater. Res.* **8**, 119–136.

Sung, L. A., Kabat, E. A. & Chien, S. 1985*a* Interaction of lectins with membrane receptors on erythrocyte surfaces. *J. Cell Biol.* **101**, 646–651.

Sung, L. A., Kabat, E. A. & Chien, S. 1985*b* Interaction energies in lectin-induced erythrocyte aggregation. *J. Cell Biol.* **101**, 652–659.

Torney, D. C., Dembo, M. & Bell, G. I. 1986 Thermodynamics of cell adhesion II: Freely mobile repellers. *Biophys. J.* **49**, 501–507.

Yamamoto, S., Hayashi, M. & Inoue, T. 1975 Viscoelastic analysis on peel adhesion of adhesive tape by matrix method. *J. appl. Polym. Sci.* **19**, 2107–2118.